Supplementary Information

Kinetically controlled narcissistic self-sorting of Pd(II)-linked self-assemblies from structurally similar tritopic ligands

Tsukasa Abe,[1] Shinnosuke Horiuchi[1] and Shuichi Hiraoka[1,*]

[1]*Department of Basic Science, Graduate School of Arts and Sciences, The University of Tokyo, 3-8-1 Komaba, Meguro-ku, Tokyo 153-8902, Japan.*

**E-mail: hiraoka-s@g.ecc.u-tokyo.ac.jp*

General Information

^{1}H, ^{13}C, ^{19}F NMR spectra were recorded using a Bruker AV-500 (500 MHz) spectrometer. All ^{1}H NMR spectra were referenced using a residual solvent peak, CD_3NO_2 (δ 4.33). Electrospray ionization time-of-flight (ESI-TOF) mass spectra were obtained using a Waters Xevo G2-S Tof mass spectrometer.

Materials

Unless otherwise noted, all solvents and reagents were obtained from commercial suppliers (TCI Co., Ltd., WAKO Pure Chemical Industries Ltd., KANTO Chemical Co., Inc., and Sigma-Aldrich Co.) and were used as received. CD_3NO_2 was purchased from Acros Organics and used after dehydration with Molecular Sieves 4Å. Tritopic ligands **1** and **2** and [***Pd***$(CH_3CN)_2$]$(PF_6)_2$ were prepared according to the literature.[1–3]

Preparation of [***Pd***Py*$_2$]$(PF_6)_2$

A solution of Py* (Py*: 3-chloropyridine) (62.5 mg, 0.55 mmol), ***Pd***Cl_2[4] (***Pd*** indicates Pd(TMEDA)) (73.5 mg, 0.25 mmol), and $AgPF_6$ (139 mg, 0.55 mmol) in anhydrous CH_3NO_2 (3 mL) was stirred at 70 °C for 3 h under nitrogen atmosphere. The obtained solution was filtered and concentrated in vacuo. The obtained solid was washed with water (1.0 mL) with a centrifugation several times to afford [***Pd***Py*$_2$]$(PF_6)_2$ as pale yellow solid in 63% yield. ^{1}H NMR (500 MHz, CD_3NO_2): δ 9.05 (d, J = 2.0 Hz, 2H), 8.98 (d, J = 5.0 Hz, 2H), 8.07 (ddd, J = 8.0, 1.5, 1.0 Hz, 2H), 7.67 (dd, J = 9.5, 5.5 Hz, 2H), 3.18 (s, 4H), 2.73 (s, 12H). ^{13}C NMR (125 MHz, CD_3NO_2): δ 152.5, 150.7, 142.7, 136.9, 130.0, 64.5, 51.8. ESI-TOF-MS (positive *m/z*): $[Pd(TMEDA)Py^*_2]^{2+}$ calcd. for $C_{16}H_{24}Cl_2N_4Pd$, 225.02; found, 225.01.

X-ray analysis of the $[\boldsymbol{Pd}_3\mathbf{1}_2]^{6+}$ cage and $(BF_4^-)\subset[\boldsymbol{Pd}_2\mathbf{1}_2]^{4+}$

The single crystals were immersed in and coated with Paraton N oil (Hampton Research Corp.) and mounted on a MicroMountTM (MiteGen LLC). Diffraction data of the single crystal were collected on a SuperNova single-crystal X-ray diffractometer with an Eos CCD detector (Rigaku Oxford Diffraction) at 180 K, using Cu Kα (λ = 1.54184 Å) radiation monochromated by multilayer mirror optics. Bragg spots were integrated using the CrysAlisPro program package (Rigaku Oxford Diffraction). An empirical absorption correction based on the multi-scan method using spherical harmonics was implemented in the SCALE3 ABSPACK scaling algorithm. The structure was solved by an intrinsic phasing method on the SHELXT program[5] and refined by a full-matrix least-squares minimization on F*2* executed by the SHELXL program[6] using the Olex2 software package (OlexSys Ltd)[7] and the ShelXle graphical user interface.[8.] The data were corrected for scattered electron density in the large solvent void by using the PLATON SQUEEZE method.[9] Thermal displacement parameters where refined anisotropically for all non-hydrogen atoms. All the hydrogen atoms were located at calculated positions and the parameters were refined with a riding model. The crystal structures are shown in Figure 3. Crystallographic data are summarized in Table S1. The data were deposited in the CSD as CCDC Deposition 2191966 for $(BF_4)\subset[\boldsymbol{Pd}_2\mathbf{1}_2](BF_4)_3$ and 2191967 for $[\boldsymbol{Pd}_3\mathbf{1}_2](PF_6)_6$, respectively.

Table S1. X-ray crystallographic data for the $[\boldsymbol{Pd}_3\mathbf{1}_2]^{6+}$ cage and $(BF_4^-)\subset[\boldsymbol{Pd}_2\mathbf{1}_2]^{4+}$.

Compound	The $[\boldsymbol{Pd}_3\mathbf{1}_2]^{6+}$ cage	$(BF_4^-)\subset[\boldsymbol{Pd}_2\mathbf{1}_2]^{4+}$
Formula	$C_{60}H_{78}F_{41}N_{12}P_7Pd_3$	$C_{56.5}H_{69.5}B_{3.5}F_{14}N_{12.5}O_5Pd_2$
Formula weight	2282.33	1520.38
Habit	colorless	colorless
Crystal size /mm	0.20 × 0.20 × 0.05	0.50 × 0.30 × 0.10
T/K	180	140
Crystal system	hexagonal	triclinic
Space group	P-62c	P-1
a/Å	16.6805(5)	12.3891(4)
b/Å	16.6805(5)	14.7381(5)
c/Å	24.1520(13)	21.5181(7)
α/°	90	98.368(3)
β/°	90	91.608(3)
γ/°	120	110.971(3)
V/Å^3	5819.7(5)	3616.0(2)
Z	2	2
d_{calc}/g · cm^{-3}	1.302	1.396
F(000)	2268	1543
μ(Cu $K\alpha$)/mm^{-1}	5.523	4.775
GOF	1.036	1.035
No. of reflns	13799	28962
Unique data	3643	13338
R_{int}	0.0509	0.0358
R_1[a] ($F^2 > 2\sigma(F^2)$)	0.0830	0.0490
wR_2[b] (all data)	0.2556	0.1420

[a] $R_1 = \Sigma||F_o| - |F_c||/\Sigma|F_o|$.

[b] $wR_2 = \{\Sigma w(F_o^2 - F_c^2)^2/\Sigma(F_o^2)^2\}^{1/2}$.

General procedure for the self-sorting experiments

A 2.4 mM solution of [2.2]paracyclophane in $CHCl_3$ (125 μL), which was used as an internal standard, was added to two NMR tubes (tubes **I** and **II**) and the solvent was removed in vacuo. A solution of [***Pd***Py*$_2$](PF$_6$)$_2$ or [***Pd***(CH$_3$CN)$_2$](PF$_6$)$_2$ solution in CD_3NO_2 was prepared as solution **A** (10 mM (for [***Pd***]$_0$ = 1.7 mM). Solution **A** (60 μL), $CDCl_3$ (50 μL), CD_3NO_2 (490 μL) were added to tube **I**. The exact concentration of [***Pd***Py*$_2$](PF$_6$)$_2$ or [***Pd***(CH$_3$CN)$_2$](PF$_6$)$_2$) in solution **A** was determined through the comparison of the signal integral with [2.2]paracyclophane by ^{1}H NMR. Solution of tritopic ligands **1** and **2** (10 mM (for [**1**]$_0$ = [**2**]$_0$ = 0.67 mM) in $CHCl_3$ (40 mL) were added to tube **II** and the solvent was removed in vacuo. Then, $CDCl_3$ (50 μL) and CD_3NO_2 (450 μL) was added to tube **II** and the exact amount of **1** in tube **II** was determined through the comparison of the signal integral with [2.2]paracyclophane by ^{1}H NMR. 1.25 eq. (against the total amounts of ligands **1** and **2** in tube **II**) of solution **A** (*ca.* 100 μL; the exact amount was determined based on the exact concentrations of solution **A** and of **1** in tube **II**) was added to tube **II**. Then, *n*-Bu$_4$N·NO$_3$ in CD_3NO_2 (20 mM, 30 μL) was added to tube **II**. After convergence monitored by ^{1}H NMR, the existence ratios of $(NO_3^-)\subset[\boldsymbol{Pd}_3\mathbf{1}_2]^{6+}$, $(NO_3^-)\subset[\boldsymbol{Pd}_2\mathbf{2}_2]^{4+}$ and $(NO_3^-)\subset[\boldsymbol{Pd}_2\mathbf{1}\cdot\mathbf{2}]^{4+}$ based on **1** and **2** were quantified by the integral value of each ^{1}H NMR signal against the signal of the internal standard ([2.2]paracyclophane). The existence ratios indicate the distribution of the two tritopic ligands in the assemblies. Thus, when the self-assembly takes place in a purely statistic manner (nonselective), the existence ratios of $(NO_3^-)\subset[\boldsymbol{Pd}_3\mathbf{1}_2]^{6+}$, $(NO_3^-)\subset[\boldsymbol{Pd}_2\mathbf{2}_2]^{4+}$ and $(NO_3^-)\subset[\boldsymbol{Pd}_2\mathbf{1}\cdot\mathbf{2}]^{4+}$ should be 50, 50 and 50%, respectively, where the ratio of the numbers of the assemblies is 1:1:2.

Characterization of the $[\boldsymbol{Pd}_3\boldsymbol{1}_2]^{6+}$ cage

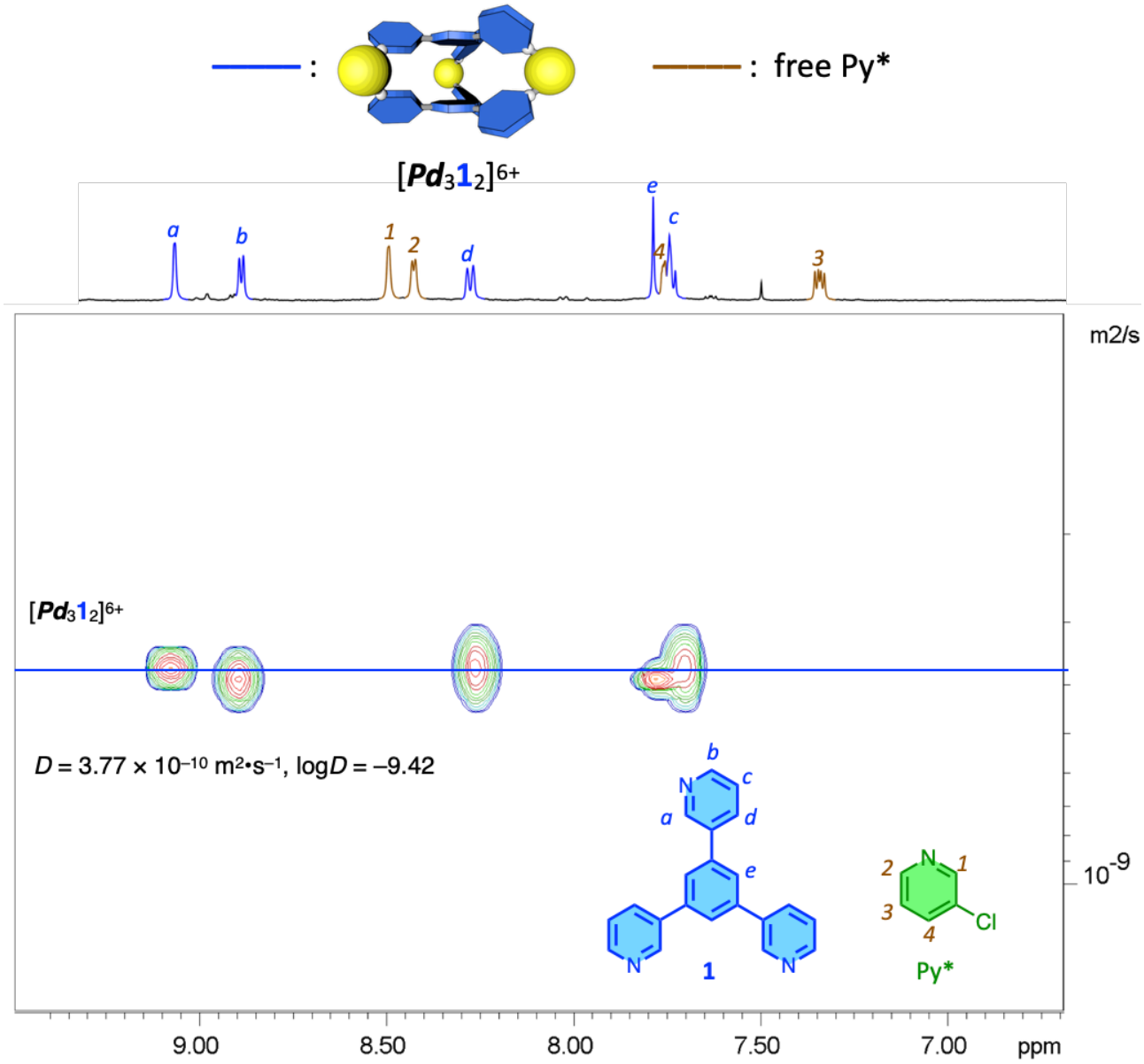

Figure S1. ^{1}H DOSY NMR spectrum (500 MHz, CD_3NO_2, 298 K, aromatic region) of the reaction mixture for the self-assembly of the $[\boldsymbol{Pd}_3\boldsymbol{1}_2](PF_6)_6$ cage from $[\boldsymbol{Pd}Py^*_2](PF_6)_2$ and **1** ($[\boldsymbol{Pd}]_0$ = 1.0 mM and $[\boldsymbol{1}]_0$ = 0.67 mM) in CD_3NO_2 at 298 K measured after convergence. The signals colored blue and brown indicate $[\boldsymbol{Pd}_3\boldsymbol{1}_2]^{6+}$ and Py*, respectively.

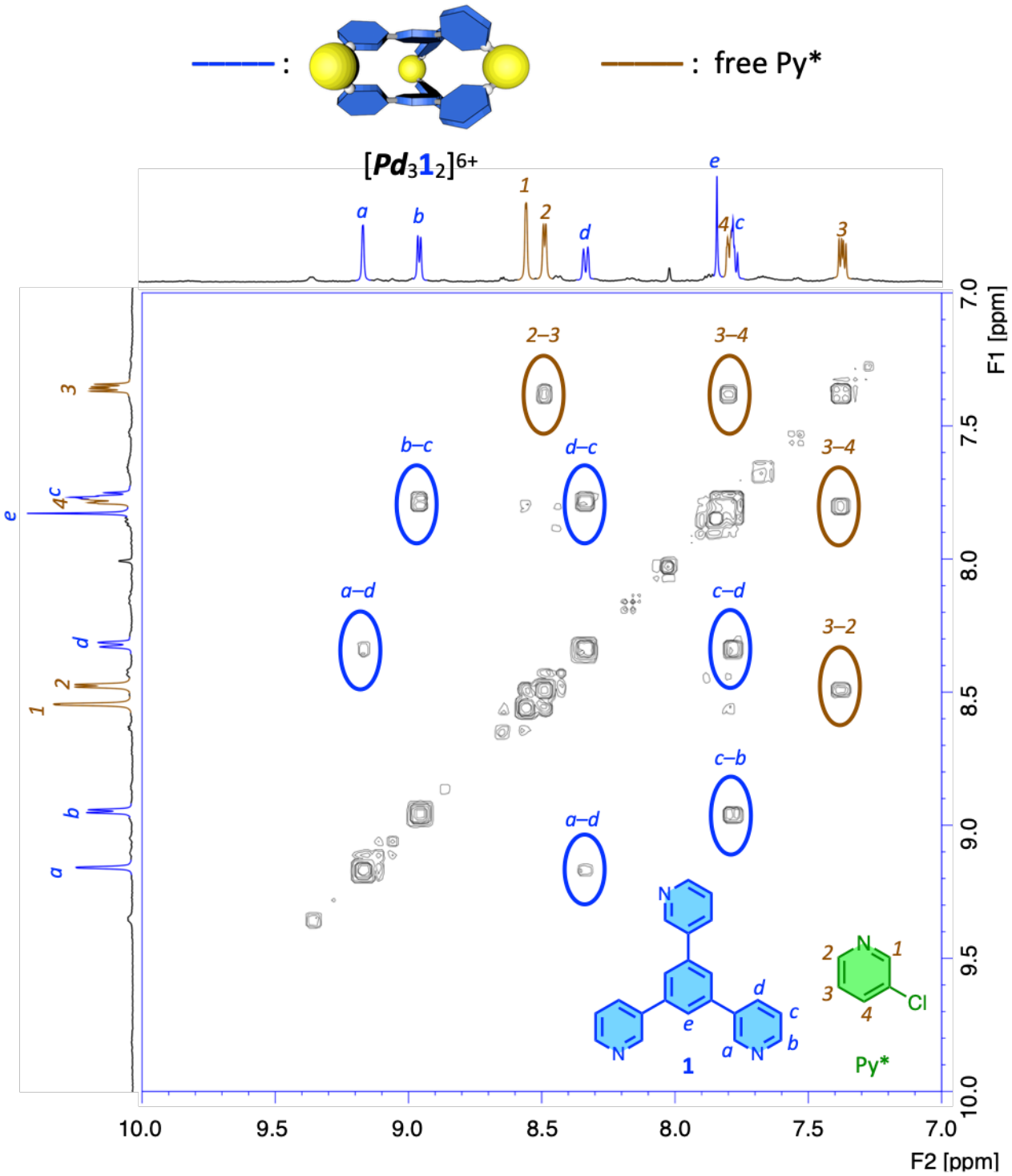

Figure S2. (H,H)-COSY NMR spectrum (500 MHz, CD_3NO_2, 298 K, aromatic region) of the reaction mixture for the self-assembly of the $[\boldsymbol{Pd}_3\mathbf{1}_2](PF_6)_6$ cage from $[\boldsymbol{Pd}Py^*_2](PF_6)_2$ and **1** ($[\boldsymbol{Pd}]_0$ = 1.0 mM and $[\mathbf{1}]_0$ = 0.67 mM) in CD_3NO_2 at 298 K measured after convergence. The signals colored blue and brown indicate $[\boldsymbol{Pd}_3\mathbf{1}_2](PF_6)_2$ cage and Py*, respectively.

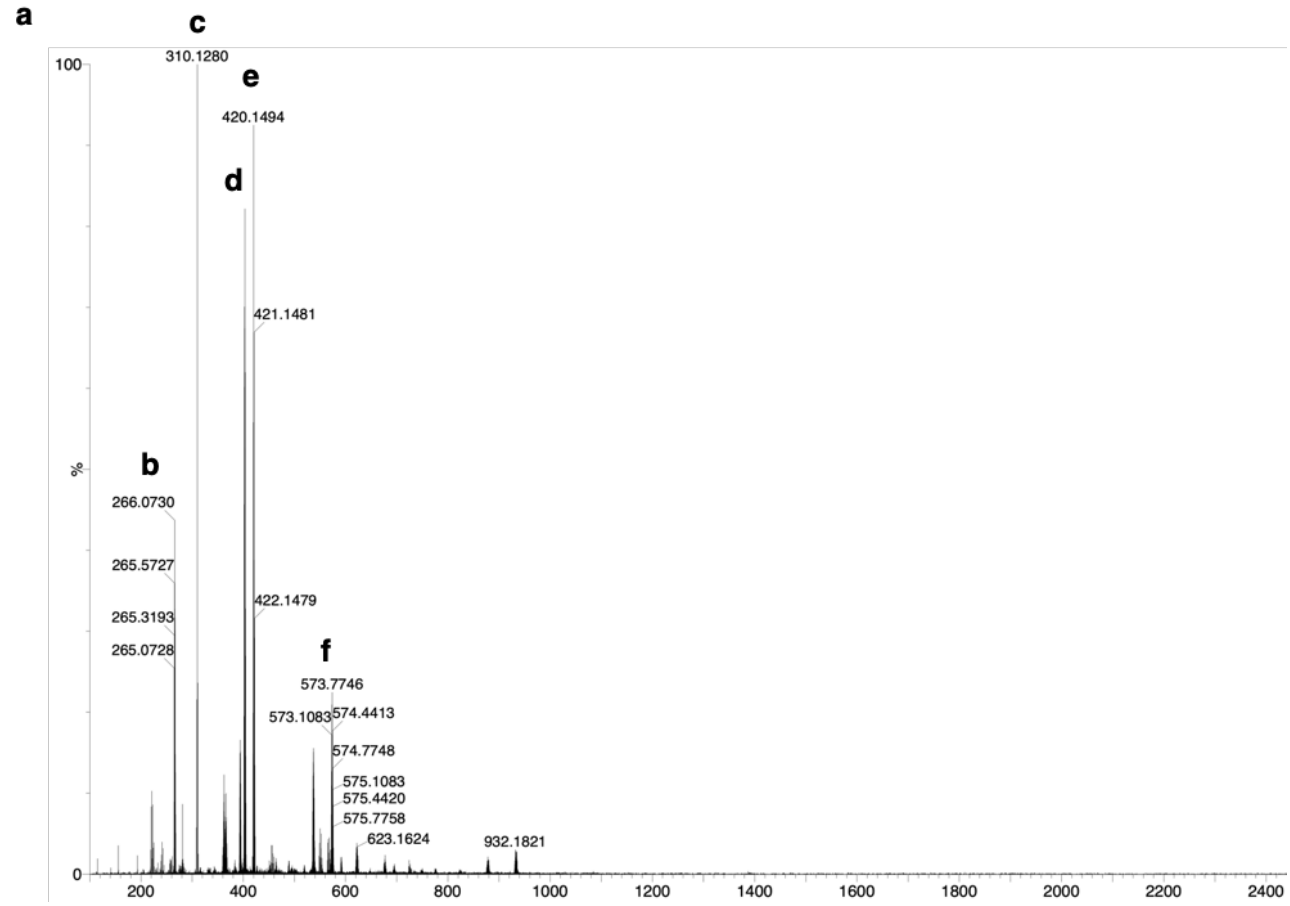
a
c
310.1280
e
420.1494
d
421.1481
b
266.0730
265.5727
422.1479
265.3193
265.0728
f
573.7746
573.1083
574.4413
574.7748
575.1083
575.4420
575.7758
623.1624
932.1821
100
%
0
200
400
600
800
1000
1200
1400
1600
1800
2000
2200
2400

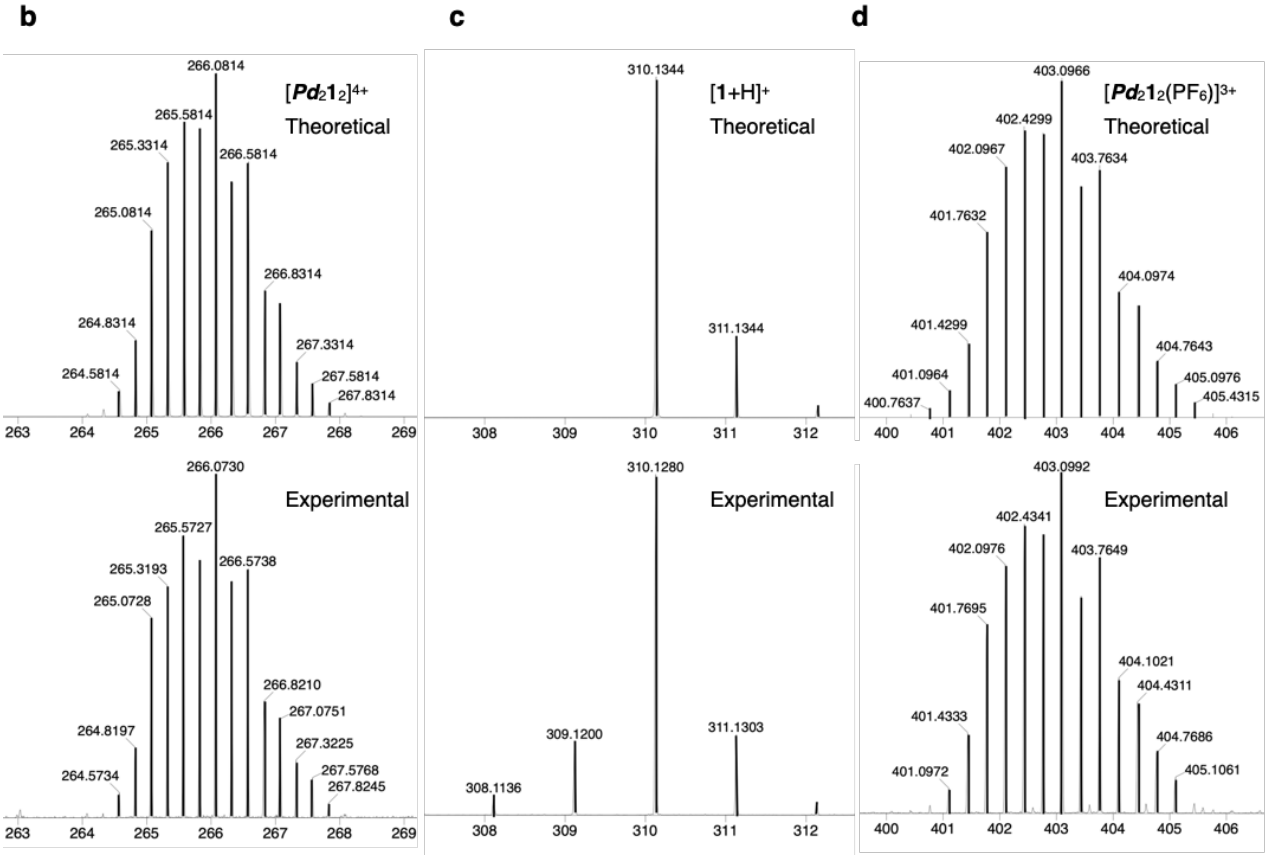
b
266.0814
[Pd21 2]4+
Theoretical
265.5814
265.3314
266.5814
265.0814
266.8314
264.8314
267.3314
264.5814
267.5814
267.8314
263
264
265
266
267
268
269
266.0730
Experimental
265.5727
265.3193
266.5738
265.0728
266.8210
267.0751
264.8197
267.3225
264.5734
267.5768
267.8245
c
310.1344
[1+H]+
Theoretical
311.1344
308
309
310
311
312
310.1280
Experimental
309.1200
311.1303
308.1136
d
403.0966
[Pd21 2(PF6)]3+
Theoretical
402.4299
402.0967
403.7634
401.7632
404.0974
401.4299
404.7643
401.0964
405.0976
400.7637
405.4315
400
401
402
403
404
405
406
403.0992
Experimental
402.4341
402.0976
403.7649
401.7695
404.1021
404.4311
401.4333
404.7686
401.0972
405.1061

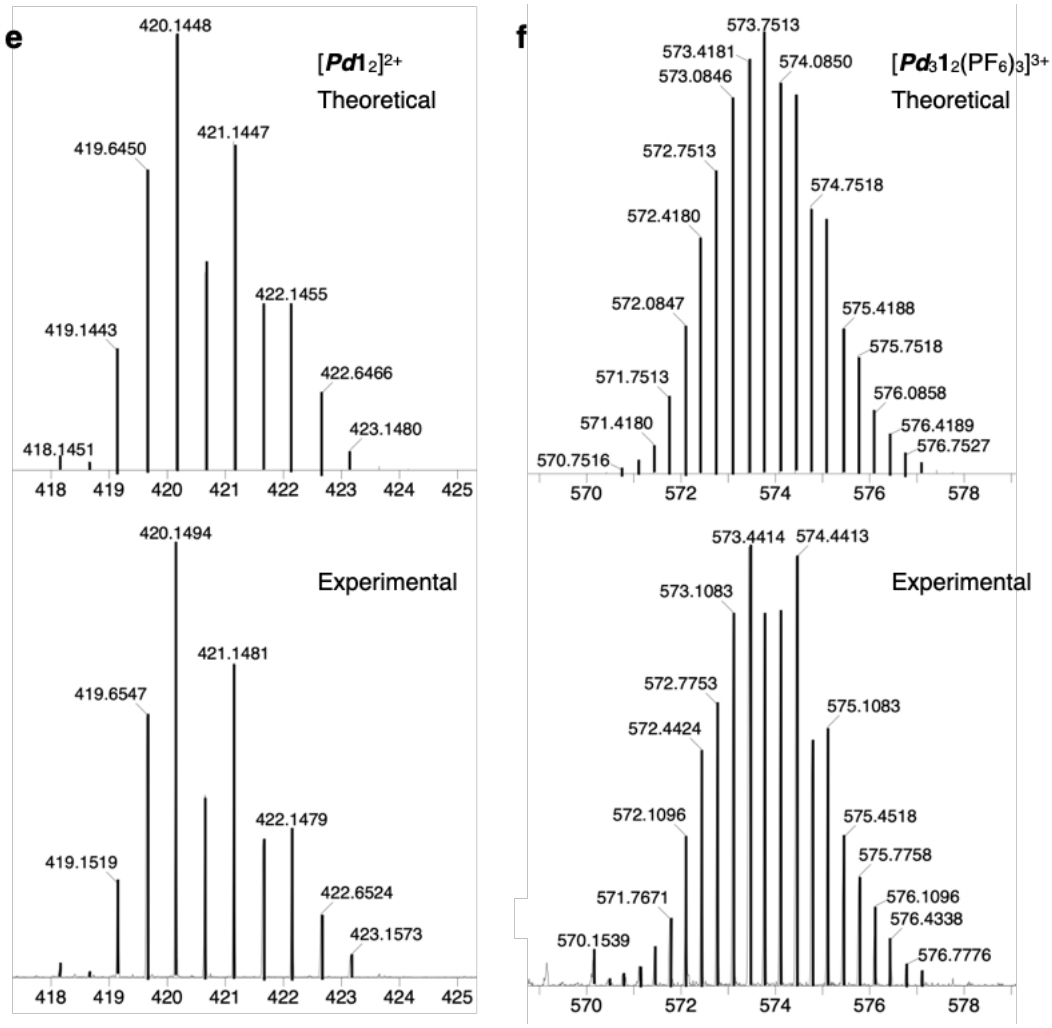

Figure S3. ESI-TOF mass spectrum of the reaction mixture for the self-assembly of the $[\boldsymbol{Pd}_3\mathbf{1}_2]^{6+}$ cage from $[\boldsymbol{Pd}\text{Py*}_2](BF_4)_2$ and **1** in CD_3NO_2 at 298 K measured after convergence. (a): overall spectrum, (b)–(f): expanded spectra.

Characterization of $(BF_4^-)\subset[\boldsymbol{Pd}_2\boldsymbol{1}_2]^{4+}$

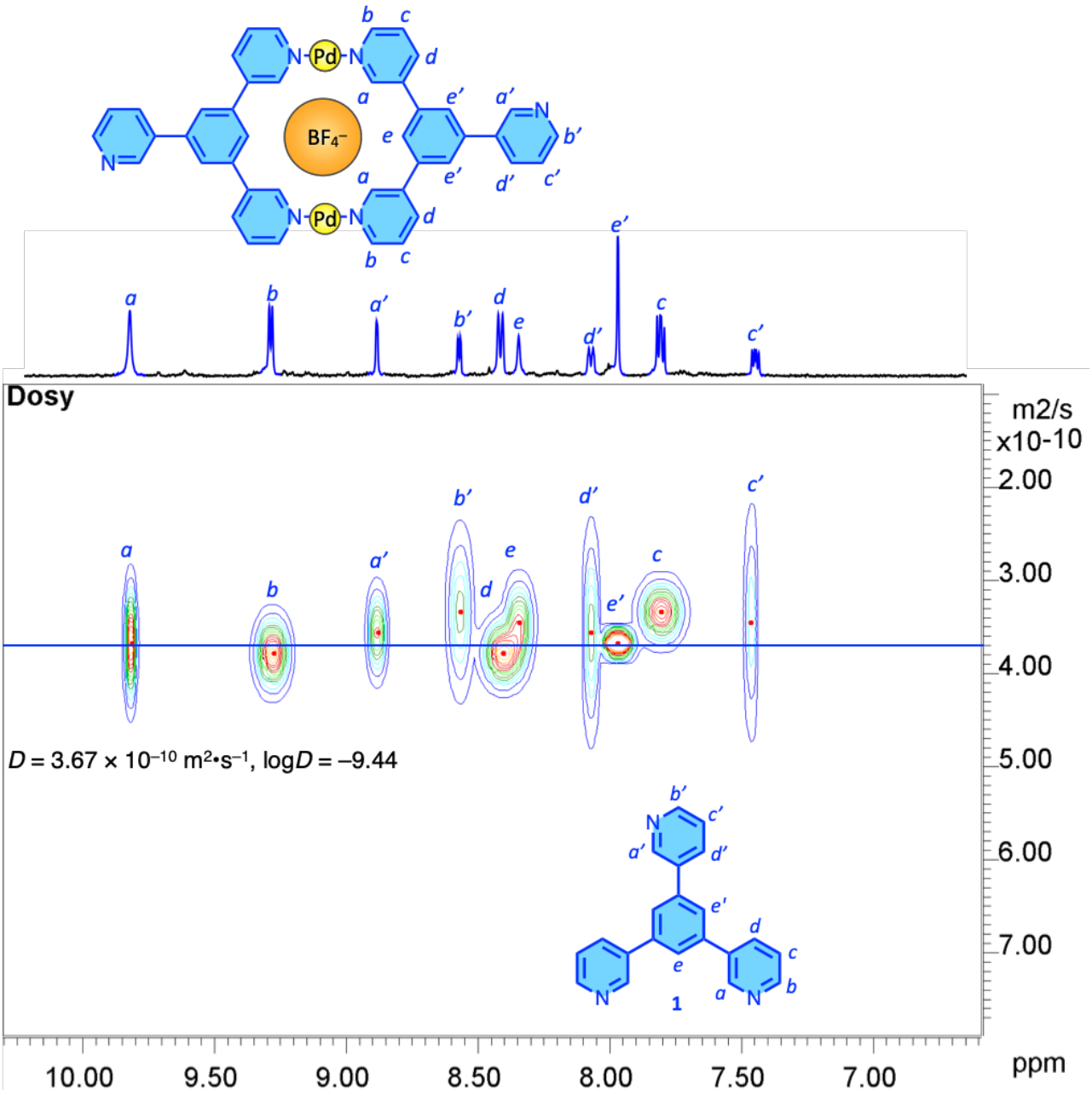

Figure S4. ^{1}H DOSY NMR spectrum (500 MHz, CD_3NO_2, 298 K, aromatic region) of $(BF_4^-)\subset[\boldsymbol{Pd}_2\boldsymbol{1}_2]^{4+}$ in CD_3NO_2 at 298 K measured after convergence. The signals colored blue indicate $(BF_4^-)\subset[\boldsymbol{Pd}_2\boldsymbol{1}_2]^{4+}$. The pyridyl rings including H^a–H^d are engaged in coordinating to a Pd(II) ion, while that including $H^{a'}$–$H^{d'}$ does not coordinate to a Pd(II) ion.

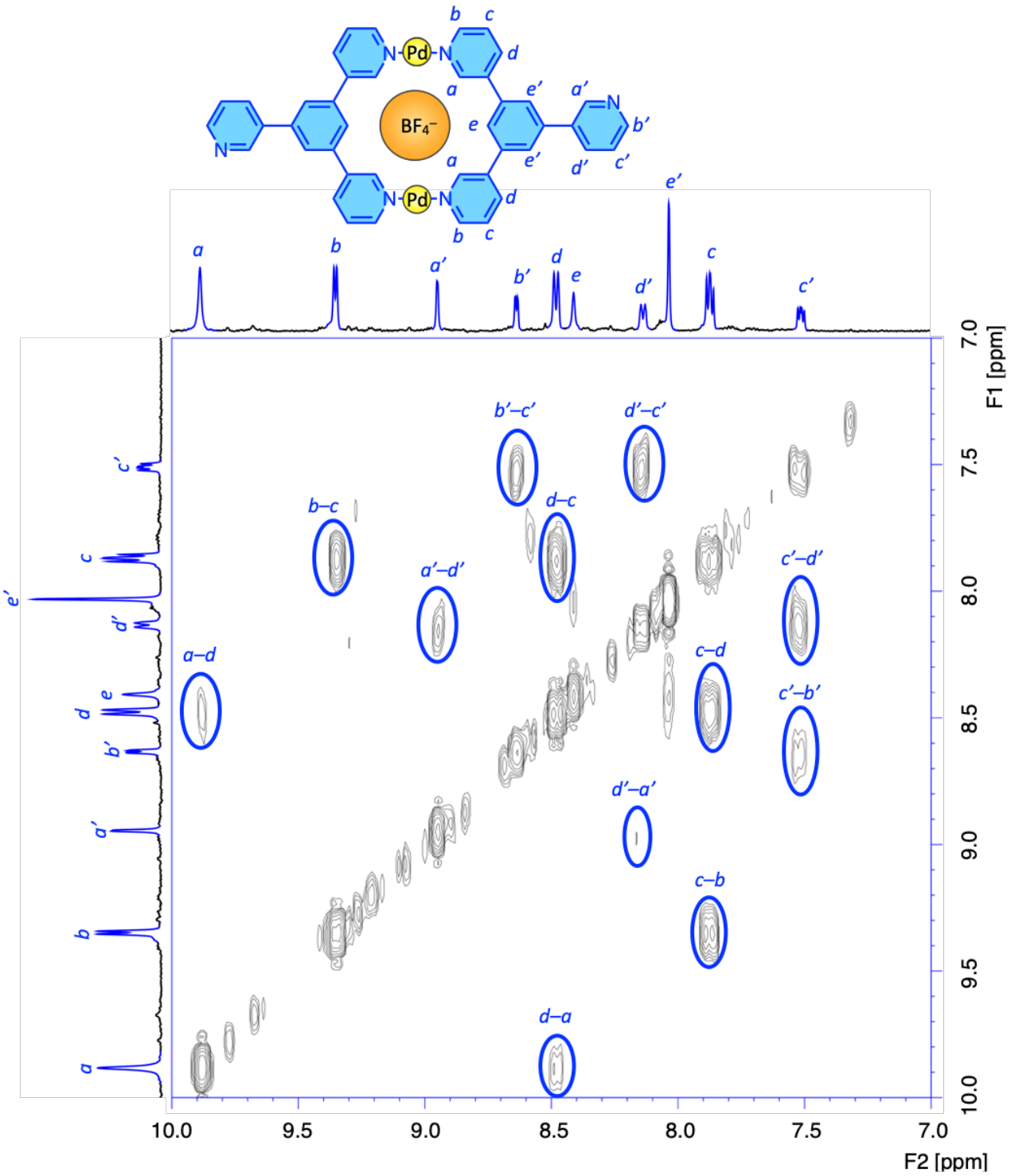

Figure S5. (H,H)-COSY NMR spectrum (500 MHz, CD_3NO_2, 298 K, aromatic region) of $(BF_4^-)\subset[\boldsymbol{Pd}_2\boldsymbol{1}_2]^{4+}$ in CD_3NO_2 at 298 K measured after convergence. The signals colored blue indicate $(BF_4^-)\subset[\boldsymbol{Pd}_2\boldsymbol{1}_2]^{4+}$. The pyridyl rings including H^a–H^d are engaged in coordinating to a Pd(II) ion, while that including $H^{a'}$–$H^{d'}$ does not coordinate to a Pd(II) ion.

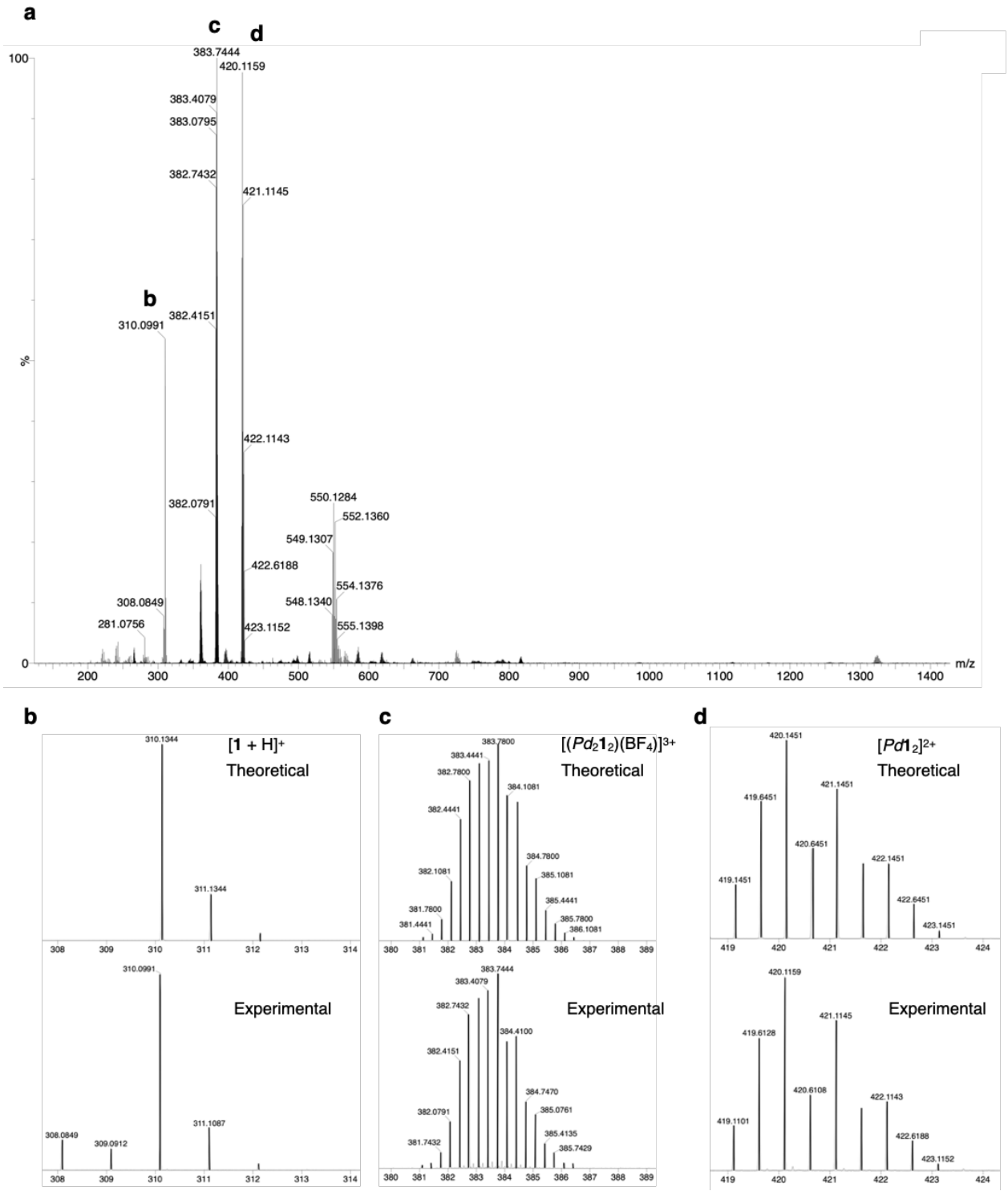

Figure S6. ESI-TOF mass spectrum of the reaction mixture for the self-assembly of $(BF_4)\subset[\boldsymbol{Pd}_2\mathbf{1}_2]^{4+}$ from $[\boldsymbol{Pd}\text{Py*}_2](BF_4)_2$ and **1** in CD_3NO_2 at 298 K measured after convergence. (a): overall spectrum, (b)–(d): expanded spectra.

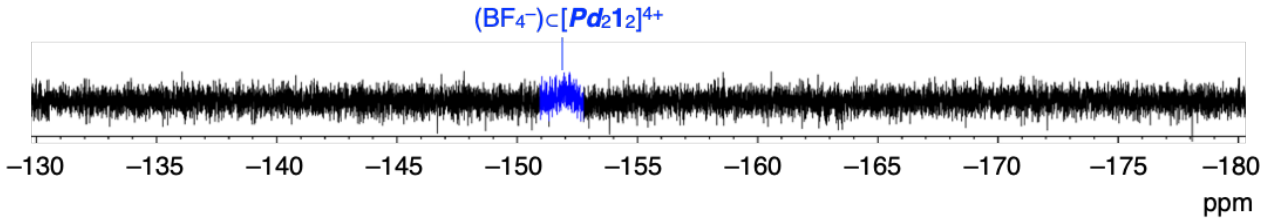

Figure S7. Partial ^{19}F NMR spectrum (500 MHz, CD_3NO_2, 298 K) of $(BF_4^-)\subset[\boldsymbol{Pd}_2\mathbf{1}_2]^{4+}$ in CD_3NO_2 measured after convergence. The signal colored in blue indicates $(BF_4^-)\subset[\boldsymbol{Pd}_2\mathbf{1}_2]^{4+}$.

Determination of the equilibrium constants between NO_3^- and the $[\boldsymbol{Pd}_3\boldsymbol{1}_2]^{6+}$ cage

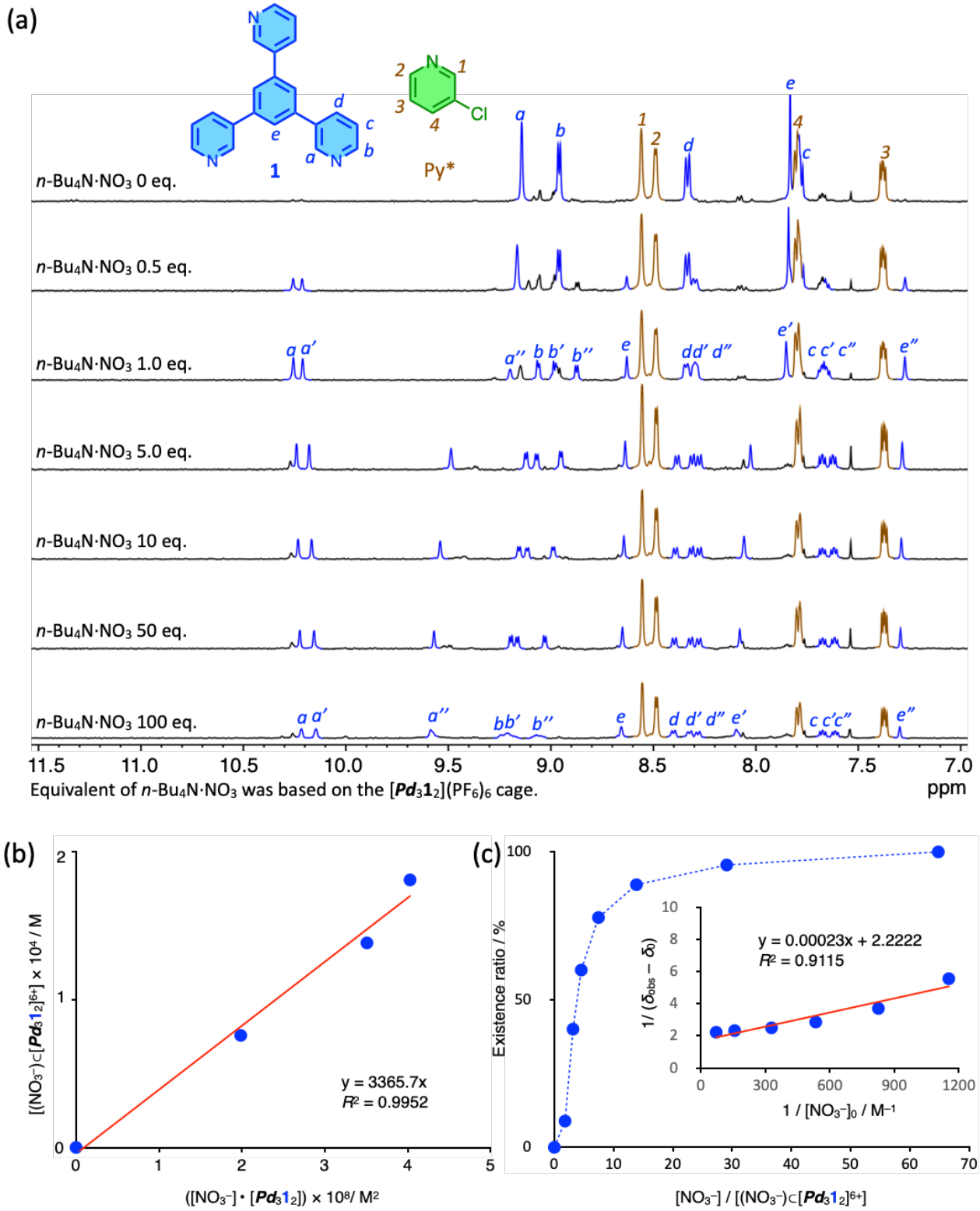

Figure S8. (a) Selected ^{1}H NMR spectra (500 MHz, CD_3NO_2, 298 K, aromatic region, $[\mathbf{1}]_0$ = 0.67 mM, $[\boldsymbol{Pd}\text{Py*}_2(PF_6)_2]$ = 1.0 mM) of the titration experiment of the $[\boldsymbol{Pd}_3\boldsymbol{1}_2](PF_6)_6$ cage with *n*-$Bu_4N{\cdot}NO_3$. Binding isotherm to determine (b) the first and (c) the second equilibrium constants between NO_3^- and the $[\boldsymbol{Pd}_3\boldsymbol{1}_2]$ cage.

Characterization of the $[\boldsymbol{Pd}_3\boldsymbol{2}_2]^{6+}$ cage

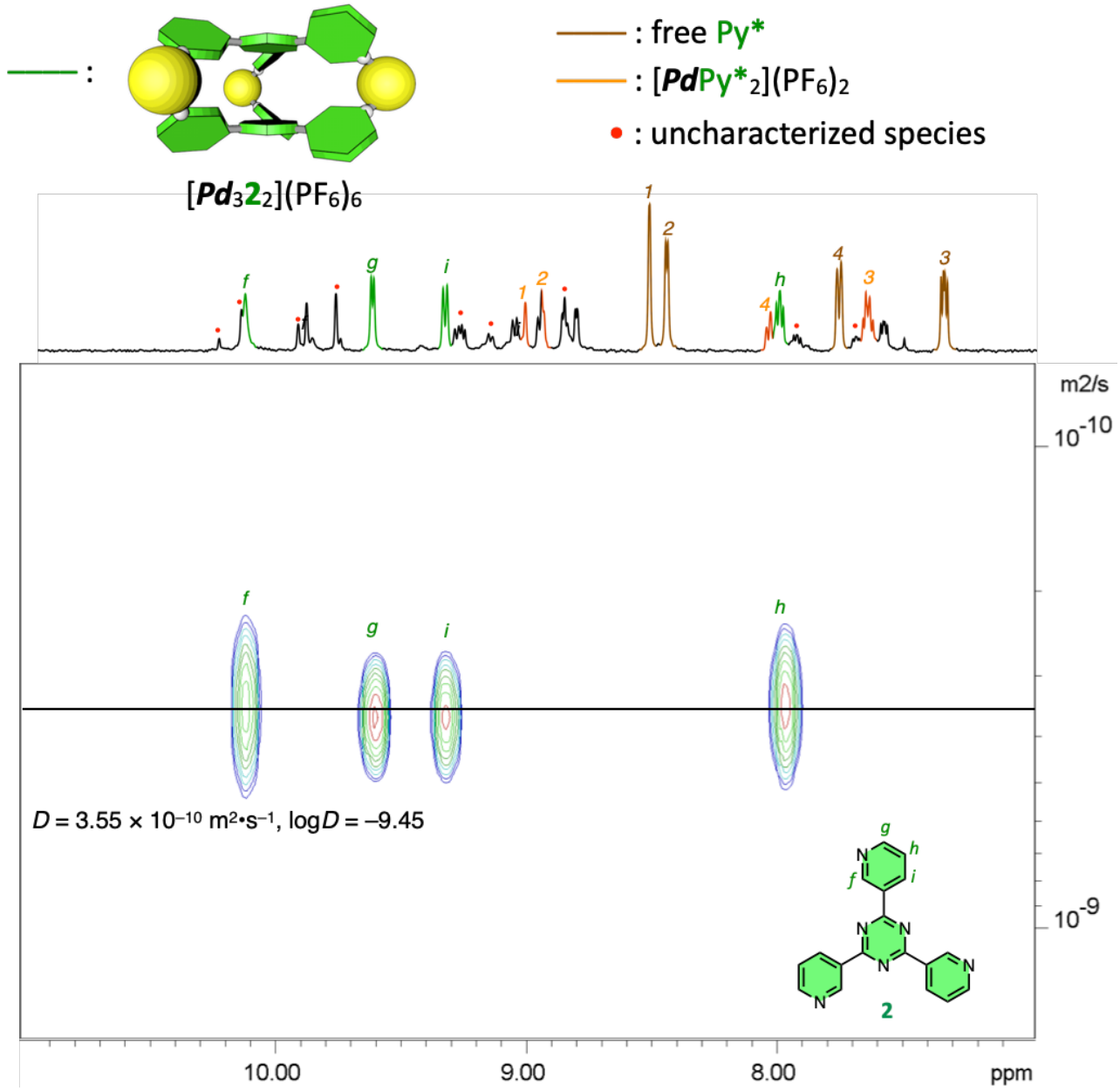

Figure S9. ^{1}H DOSY NMR spectrum (500 MHz, CD_3NO_2, 298 K, aromatic region) of the reaction mixture for the self-assembly of the $[\boldsymbol{Pd}_3\boldsymbol{2}_2](PF_6)_6$ cage from $[\boldsymbol{Pd}Py^*_2](PF_6)_2$ and **2** ($[\boldsymbol{Pd}]_0$ = 0.82 mM and $[\boldsymbol{2}]_0$ = 0.82 mM) in CD_3NO_2 at 298 K measured after convergence. The signals colored green, brown, and orange indicate the $[\boldsymbol{Pd}_3\boldsymbol{2}_2](PF_6)_6$ cage, Py*, and $[\boldsymbol{Pd}Py^*_2](PF_6)_2$, respectively. The signals marked in red solid circle indicate the uncharacterized species.

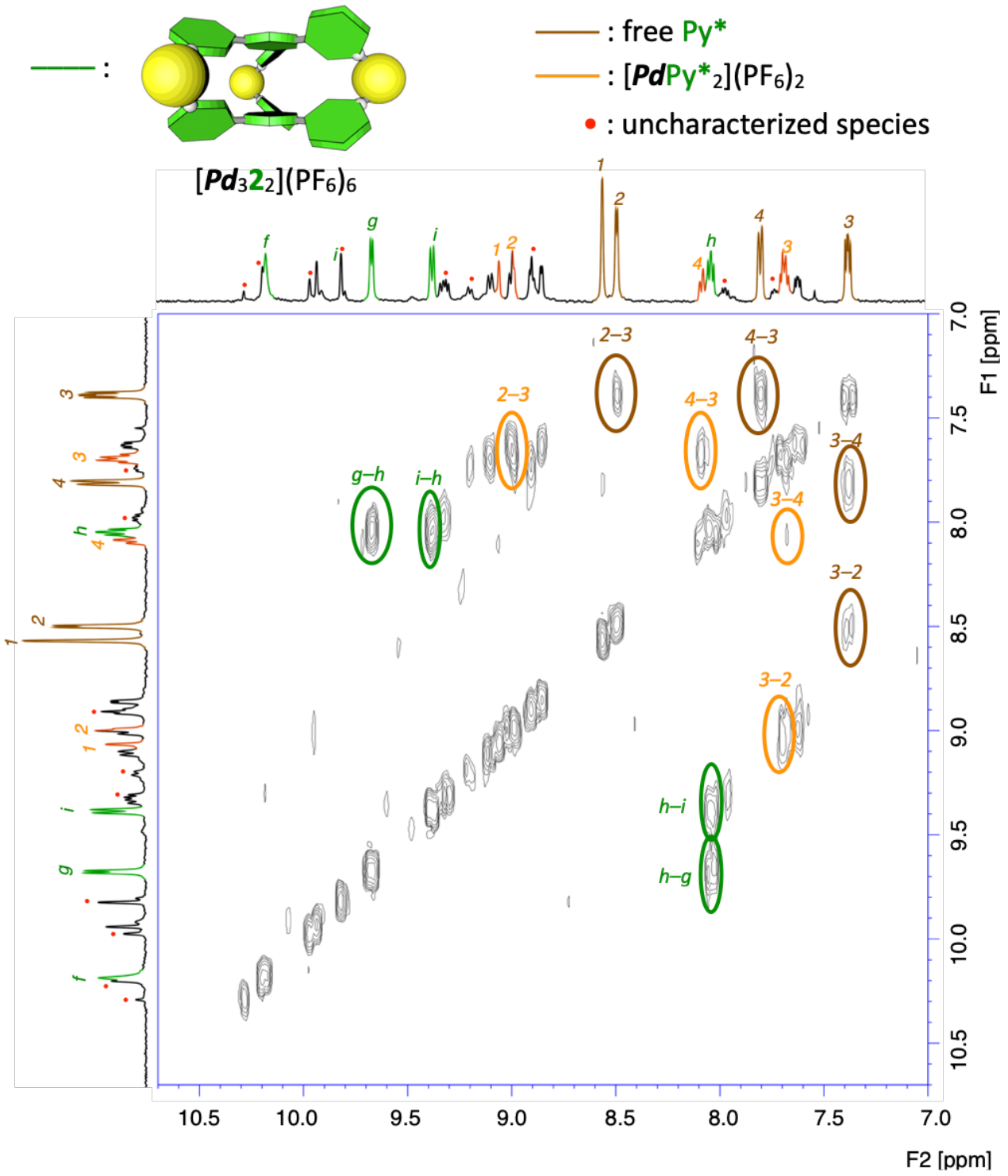

Figure S10. (H,H)-COSY NMR spectrum (500 MHz, CD_3NO_2, 298 K, aromatic region) of the reaction mixture for the self-assembly of the $[\boldsymbol{Pd}_3\mathbf{2}_2](PF_6)_6$ cage from $[\boldsymbol{Pd}Py^*_2](PF_6)_2$ and **2** ($[\boldsymbol{Pd}]_0$ = 0.82 mM and $[\mathbf{2}]_0$ = 0.82 mM) in CD_3NO_2 at 298 K measured after convergence. The signals colored green, brown, and orange indicate the $[\boldsymbol{Pd}_3\mathbf{2}_2](PF_6)_6$ cage, Py*, and $[\boldsymbol{Pd}Py^*_2](PF_6)_2$, respectively. The signals marked in red solid circle indicate the uncharacterized species.

Assignment of the ^{1}H NMR spectra of $(X^-)\subset[\boldsymbol{Pd_2}\mathbf{2}_2]^{4+}$

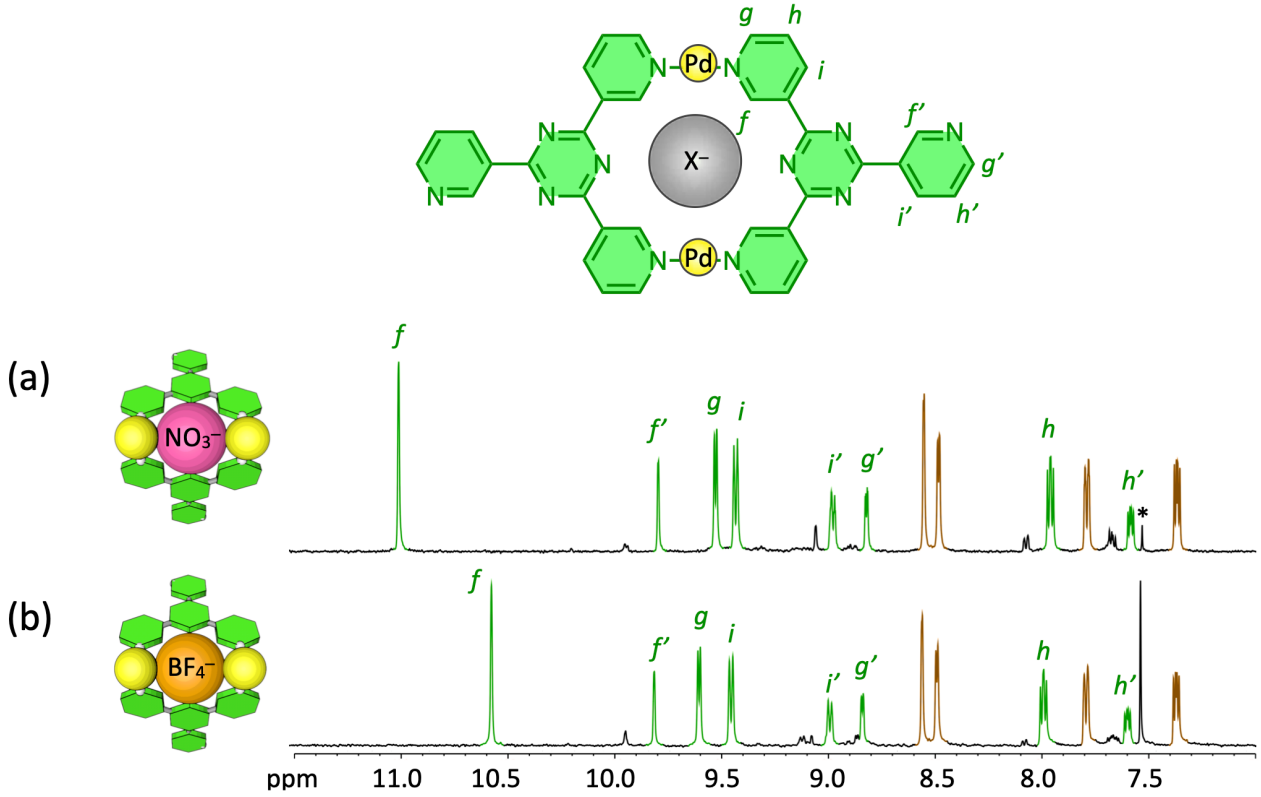

Figure S11. ^{1}H NMR spectra of (a) $(NO_3^-)\subset[\boldsymbol{Pd_2}\mathbf{2}_2]^{4+}$ and (b) $(BF_4^-)\subset[\boldsymbol{Pd_2}\mathbf{2}_2]^{4+}$ with their assignments.

^{1}H NMR spectra of the self-sorting experiments

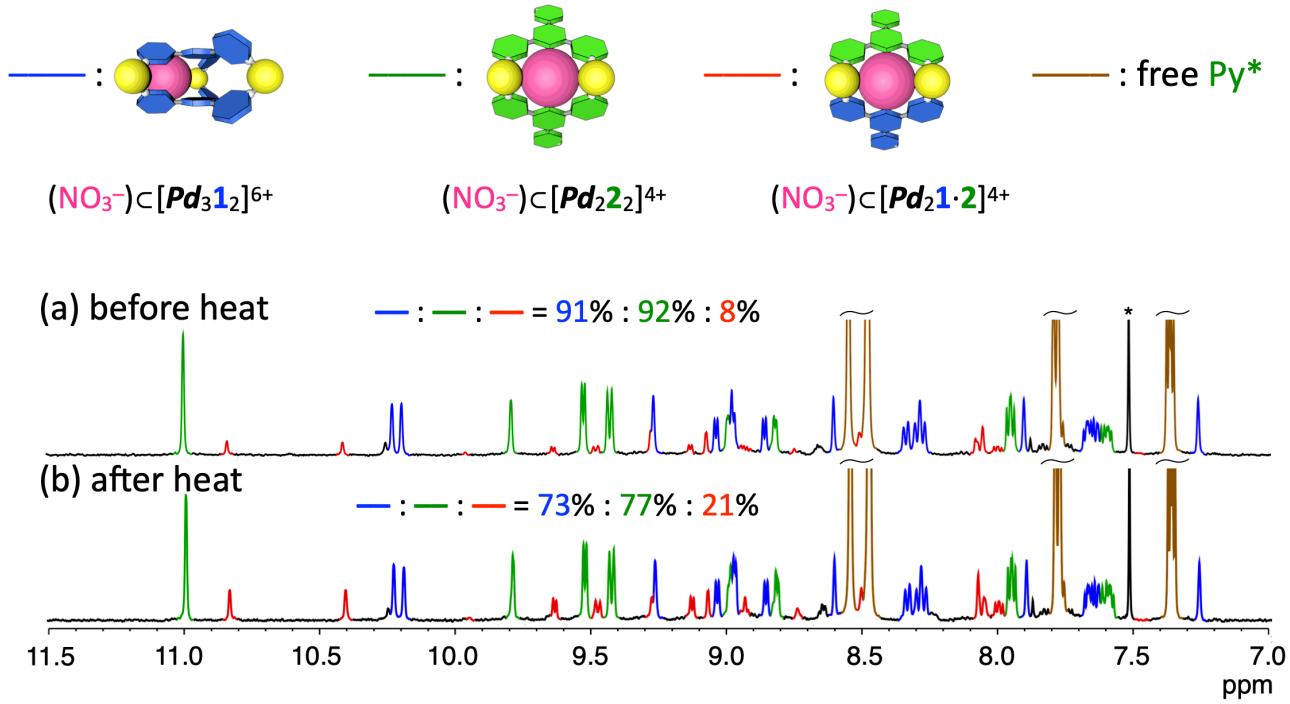

Figure S12. ^{1}H NMR spectra (500 MHz, CD_3NO_2:$CDCl_3$ = 11:1 (v/v), 298 K, aromatic region, $[\mathbf{1}]_0 = [\mathbf{2}]_0$ = 0.67 mM, [***Pd***Py*$_2$$(PF_6)_2$] = 1.0 mM) of the self-sorting experiments of (a) state III and (b) state II generated from state III by heating to reach equilibrium.

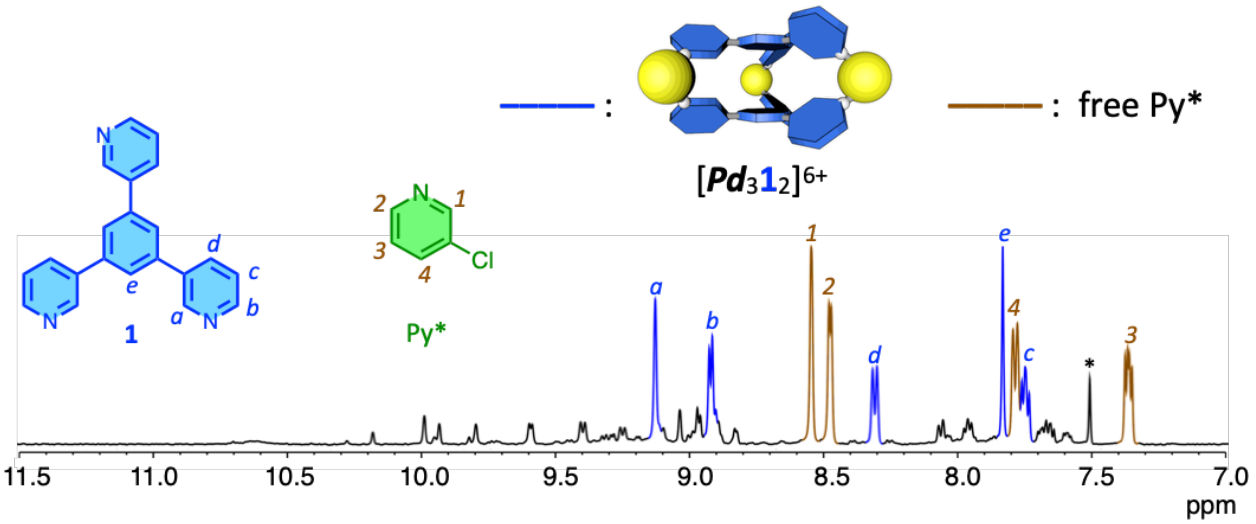

Figure S13. ^{1}H NMR spectrum (500 MHz, CD_3NO_2:$CDCl_3$ = 11:1 (v/v), 298 K, aromatic region, $[\mathbf{1}]_0 = [\mathbf{2}]_0$ = 0.67 mM, [***Pd***Py*$_2$$(PF_6)_2$] = 1.0 mM) of the reaction mixture of **1**, **2**, and [***Pd***Py*$_2$](PF$_6$)$_2$ at 363 K. Signals in blue and brown are assigned to the [***Pd***$_3$**1**$_2$](PF$_6$)$_6$ cage and free Py*, respectively.

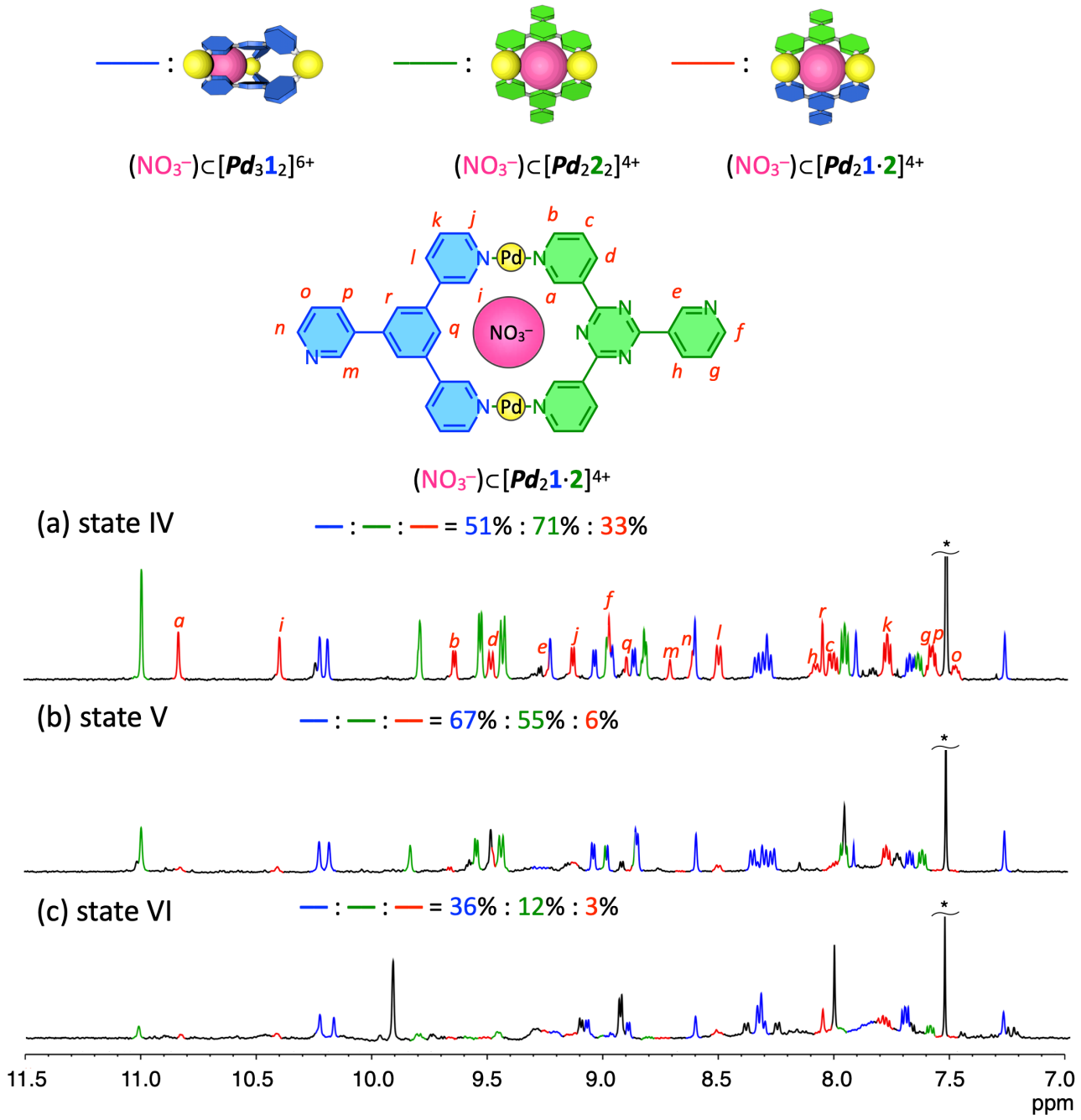

Figure S14. ^{1}H NMR spectra (500 MHz, CD_3NO_2:$CDCl_3$ (11:1 (v/v)), 298 K, aromatic region) of the self-sorting experiments depending on the pathway using CH_3CN as a leaving ligand. (a) state IV generated at 298 K by initially adding NO_3^-. The assignment of the signals of $(NO_3^-)\subset[\boldsymbol{Pd_2}\mathbf{1}\cdot\mathbf{2}]^{4+}$ is indicated by red characters. (b) state V generated from states IV and VI by heating to reach equilibrium. (c) state VI generated at 363 K without NO_3^-, following that NO_3^- was added at 298 K. The assignment of the signals for $(NO_3^-)\subset[\boldsymbol{Pd_3}\mathbf{1}_2]^{6+}$ and $(NO_3^-)\subset[\boldsymbol{Pd_2}\mathbf{2}_2]^{4+}$ are shown in Figures S2 and S11a, respectively. Asterisk indicates $CHCl_3$.

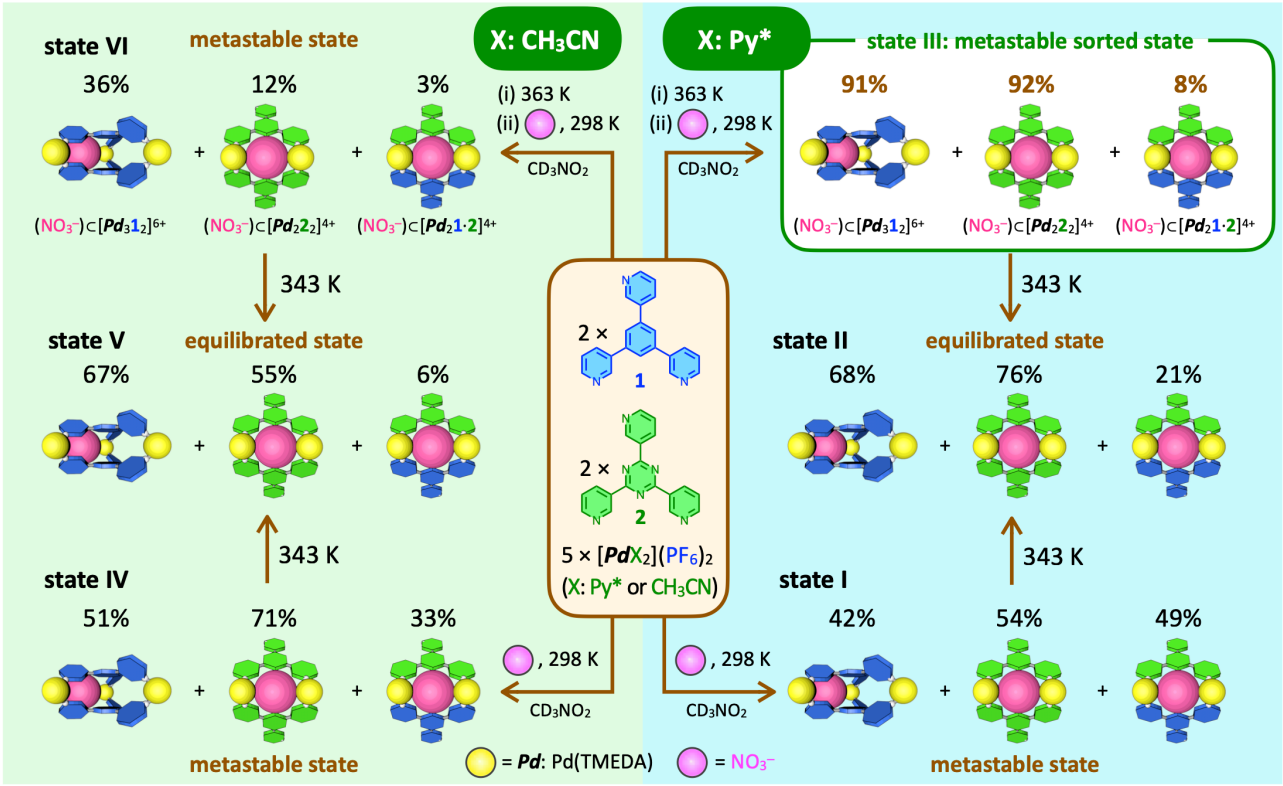

Figure S15. A summary of the self-sorting experiments of the tritopic ligands **1** and **2** with [***Pd***X_2]$(PF_6)_2$ in CD_3NO_2.

References

1. R. Lavendomme, T. K. Ronson and J. R. Nitschke, *J. Am. Chem. Soc.* 2019, **141**, 12147–12158.
2. H. L. Anderson, S. Anderson and J. K. M. Sanders, *J. Chem. Soc. Perkin Trans. 1* 1995, 2231–2245.
3. K. Uehara, T. Oishi, T. Hirose and N. Mizuno, *Inorg. Chem.* 2013, **52**, 11200−11209.
4. F. Proutiere, E. Lyngvi, M. Aufiero, I. A. Sanhueza and F. Schoenebeck, *Organometallics* 2014, **33**, 6879–6884.
5. G. M. Sheldrick, *Acta Crystallogr. Sect. A* 2015, **71**, 3–8.
6. G. M. Sheldrick, G. M. *Acta Crystallogr. Sect. C* 2015, **71**, 3–8.
7. O. V. Dolomanov, L. J. Bourhis, R. J. Gildea, J. A. K. Howard and H. Puschmann, *J. Appl. Crystallogr.* 2009, **42**, 339–341.
8. C. B. Hübschle, G. M. Sheldrick, B. Dittrich, *ShelXle*: a Qt graphical user interface for *SHELXL*. *J. Appl. Cryst.* 2011, **44**, 1281–1284.
9. A. L. Spek, *Acta Crystallogr. Sect. D* 2009, **65**, 148–155.